

SnSe monolayer: Super-flexible, auxetic material with ultralow lattice thermal conductivity and ultrahigh hole mobility

*Li-Chuan Zhang,[†] Guangzhao Qin,[†] Wu-Zhang Fang,[‡] Hui-Juan Cui,[‡] Qing-Rong Zheng,[‡]
Qing-Bo Yan,^{*,†} Gang Su^{*,‡}*

[†]College of Materials Science and Opto-Electronic Technology, University of Chinese Academy of Sciences, Beijing, China 100049;

[‡]School of Physical Sciences, University of Chinese Academy of Sciences, Beijing, China 100049

KEYWORDS: SnSe monolayer, auxetic material, hole mobility, strain engineering, first-principles calculations

ABSTRACT: By performing extensive first-principles calculations, we found that SnSe monolayer is an indirect band gap (~ 1.45 eV) semiconductor with amazing properties, including a large negative Poisson's ratio (-0.17), a very low lattice thermal conductivity ($< 3 \text{ Wm}^{-1}\text{K}^{-1}$), and a high hole mobility (of order $10000 \text{ cm}^2\text{V}^{-1}\text{S}^{-1}$). In contrast to phosphorene with a similar hinge-like structure, SnSe monolayer has unexpectedly symmetric phonon and electronic structures, and nearly isotropic lattice thermal conductivity and carrier effective mass. However, the electronic responses to strain are sensitive and anisotropic, leading to indirect-direct band gap transitions under a rather low strain (< 0.5 GPa) and a highly anisotropic carrier mobility. These

intriguing properties make monolayer SnSe a promising two-dimensional material for nanomechanics, thermoelectrics, and optoelectronics.

Introduction

The discovery of graphene leads to an upsurge in exploring two-dimensional (2D) materials¹⁻⁵, such as hexagonal boron nitride⁶⁻⁷, transition metal dichalcogenides (TMDCs)⁸⁻⁹, silicene¹⁰, germanene^{11,12}, and others¹³. Recently, few-layer black phosphorus has been successfully exfoliated, arousing wide interest for researchers¹⁴⁻²⁰. Single layer black phosphorus (phosphorene) was found to be a novel 2D direct band gap semiconductor with anisotropic carrier mobility and other properties, leading phosphorene to be a promising candidate in nanoelectronics²¹. Bulk tin selenide (SnSe) has a hinge-like layered structure similar to black phosphorous²²⁻²⁸, and may have applications in thermoelectric devices²⁶, memory switching²⁷, and optoelectronics²⁹. Very recently, 2D SnSe has been synthesized²⁹⁻³¹, which is expected to be useful with great potential in photodetector and photovoltaic devices. However, the physical properties of monolayer SnSe, in particular the carrier mobility, lattice thermal conductivity, strain effects, etc., are still less known.

In this paper, we systematically investigated the geometrical, mechanical, electronic properties of monolayer SnSe by utilizing the density functional theory (DFT) based first-principles calculations. We found that SnSe monolayer is a semiconductor with an indirect band gap of 1.45 eV, a very low lattice thermal conductivity below $3 \text{ Wm}^{-1}\text{K}^{-1}$, a large negative Poisson's ratio of -0.17, and a hole mobility as high as $16000 \text{ cm}^2\text{V}^{-1}\text{S}^{-1}$. In contrast to phosphorene, which was reported to have strong anisotropic mechanical, electronic, and optical properties¹⁴, SnSe monolayer was found to bear nearly symmetric phonon and electronic band structures, and other

isotropic properties, such as lattice thermal conductivity and effective mass of charge carrier, etc. Such unexpected isotropy can be attributed to its effective symmetric bilayer square-like lattice structure. The strain effect on SnSe monolayer was also studied, showing that the geometric, mechanic and electronic properties are sensitive to the strain. The calculated Young's elastic modulus are 24.3 GPa and 43.5 GPa along the armchair and zigzag direction, respectively, which may be the most flexible in known 2D materials. A very low stress (1.59 GPa) along armchair direction can induce a geometrical phase transition. Besides, a uniaxial strain will shift the extremes of different energy valleys asynchronously, giving rise to an indirect-direct band gap transition under a rather low stress (< 0.5 GPa). Although the effective mass of charge carrier is nearly isotropic, the carrier mobility is highly anisotropic, which can be attributed to the anisotropic response of electronic structure to strain. With these intriguing properties, SnSe monolayer could have wide potential applications in nanomechanics, thermoelectrics, and optoelectronics.

Results and Discussion

Geometric and mechanical properties of SnSe monolayer

Monolayer SnSe and phosphorene are isoelectronic if only valence electrons are considered. They have similar hinge-like layered structures (Fig. 1), which can be viewed as a deformed honeycomb structure of graphene. This hinge-like structure is distinctly different along armchair (x) and zigzag (y) directions, which leads to strong anisotropic properties of phosphorene^{14,16-17,32-35}. Owing to structural similarity, it is interesting to compare monolayer SnSe and phosphorene. For monolayer SnSe, the lattice parameters are $a = 4.41$ Å and $b = 4.27$ Å along x and y directions, respectively, while for phosphorene $a = 4.58$ Å and $b = 3.32$ Å, exposing that

the difference between a and b for monolayer SnSe is small, while for phosphorene it is drastic. As shown in Fig. 1b and 1c, the bond angles of Sn-Se-Sn or Se-Sn-Se are nearly 90° , while the corresponding angles of phosphorene are much larger. Monolayer SnSe is composed of two different types of elements, and phosphorene contains only one element, thus the latter is more symmetric than former. The binding energy of monolayer SnSe with respect to bulk SnSe crystal is evaluated as $32 \text{ meV}/\text{\AA}^2$, which is larger than graphene ($17.8 \text{ meV}/\text{\AA}^2$) but close to phosphorene ($29.9 \text{ meV}/\text{\AA}^2$) (see supporting materials), revealing that SnSe is more difficult to be exfoliated than graphene, but can be synthesized using similar methods to phosphorene.

The phonon dispersion of monolayer SnSe is shown in Fig. 2a. No imaginary frequency is observed, indicating its kinetic stability. Interestingly, the phonon band profile show dramatically symmetry along $\Gamma - X$ and $\Gamma - Y$ directions. From the slope of longitudinal acoustic phonon branch at Γ point, the sound speed (phonon group velocity) along $\Gamma - X$ (armchair) and $\Gamma - Y$ directions (zigzag) can be extracted as 2.9 and 3.1 km/s, respectively, which are nearly isotropic and much slower than that of phosphorene (4.0 and 7.8 km/s)¹⁶. The maximal frequency is 5.2 THz, only about 40% of phosphorene¹⁶, implying that monolayer SnSe is much softer than phosphorene. By means of phonon Boltzmann transport equation³⁶ and DFT, the lattice thermal conductivity (LTC) is calculated, as depicted in Fig. 2b. The LTC of monolayer SnSe at 300 K along x and y directions are 2.6 and 3.0 $\text{Wm}^{-1}\text{K}^{-1}$, respectively, illustrating a nearly isotropic phonon transport properties, which is lower than and contrary to the anisotropic thermal lattice conductivity of phosphorene (14 and 30 $\text{Wm}^{-1}\text{K}^{-1}$)¹⁶. Among most of the 2D materials that LTC had been studied³⁷⁻³⁹, monolayer SnSe may have the lowest LTC, implying its great potential for a good 2D thermoelectric material.

Electronic structure of monolayer SnSe

Figure 2c shows the electronic band structure of monolayer SnSe. Similar to the phonon band structure, the electronic structure also exhibits obvious symmetry along $\Gamma - X$ and $\Gamma - Y$ directions. The valence band maximum (VBM) and conduction band minimum (CBM) are marked with C_X , C_Y , V_X , V_Y , which locate at X' and Y' on $\Gamma - X$ and $\Gamma - Y$ lines (inset of Fig. 2c), respectively. At first glance, C_X and C_Y , V_X and V_Y have the same energy, respectively. However, a closer inspection reveals a small but obvious deviation. V_X is higher than V_Y about 0.20 eV, and C_Y is lower than C_X about 0.04 eV, and therefore, V_X is the valence band top (VBT) and C_Y is the conduction band bottom (CBB), indicating that monolayer SnSe is a semiconductor with an indirect gap of 1.45 eV. Various calculation methods are used to recheck this result, all of which support the observation of an indirect band gap (see supporting materials). The direct gaps between V_X and C_X , V_Y and C_Y are 1.49 and 1.65 eV, respectively. The effective mass of charge carriers can be extracted from the high-precise energy band calculation, as shown in Fig. 2d. The red solid and blue dash lines represent the effective mass of electron and hole, respectively, which are nearly a perfect circle, suggesting that the effective mass of them are nearly isotropic. As listed in Table I, the effective mass along $\Gamma - X$ and $\Gamma - Y$ are 0.14(e), 0.16(h) and 1.18(e), 0.16(h), respectively, indicating that effective mass of hole are slightly larger than that of electron. Note that the carrier effective mass of phosphorene¹⁴ along $\Gamma - X$ and $\Gamma - Y$ are 0.17(e), 0.15(h) and 1.12(e), 6.35(h), respectively, showing an obvious anisotropy.

Despite of the similar hinge-like structure of monolayer SnSe and phosphorene, we have observed unexpected nearly symmetric phonon and electronic band structures and isotropic lattice thermal conductivity and effective mass of charge carriers, in sharp contrast to the strongly anisotropic properties of phosphorene. Let us reexamine the geometrical structure of

monolayer SnSe. Each Sn (Se) atom is surrounded by five Se (Sn) atoms, three of which are bonded with bond length about 2.90 Å (horizontal bond), while other two are nonbonding neighbor atoms with Sn-Se distance of 3.26 Å, only about 11% longer than Sn-Se bond length (See supporting material). Recall that the lattice parameters along x and y directions are almost the same and the bond angles of Sn-Se-Sn or Se-Sn-Se are around 90°, and a square-like 2D lattice is actually formed (Fig. 1d), which appears to be nearly symmetric along x and y directions. In addition, the electron density (Fig. 1e) and the electrostatic potential (see supporting materials) in the plane that contains all Sn atoms of monolayer SnSe are extracted, which exhibits a character of nearly symmetric square lattice. The geometrical structure of monolayer SnSe is thus more symmetric than what we have seen in Fig. 1a, and in fact, an effectively square-like 2D lattice with hidden symmetry emerges. It implies that the ball-stick model sometimes could mislead our understanding on the geometrical structure of monolayer SnSe. A high electron density is found between the nonbonding neighboring Sn and Se atoms, revealing strong nonbonding interactions exist between them, which are weaker than Sn-Se bond, but may be still much stronger than common van der Waals interaction, otherwise the effectively square-like 2D lattice cannot be formed and the symmetric phonon and electronic band structures cannot appear. Note that the distance (3.41 Å) between nonbonding neighboring P atoms in phosphrene is about 50% longer than P-P bond length (2.28 Å), which is too long to form strong nonbonding interactions.

Strain effect on mechanical properties of monolayer SnSe

The strain effect on geometric, mechanical and electronic properties of monolayer SnSe is extensively studied. The related geometric parameters of monolayer SnSe under uniaxial strains are shown in Fig. 3, in which ϵ_x , ϵ_y , and ϵ_z indicate the relative strain along x , y and z directions,

respectively, and the negative (positive) values represent compressive (tensile) strain. It is found that the layer thickness c (along z direction) increases with the increase of lattice parameter a (along x direction), giving rise to a negative Poisson's ratio of -0.17, showing that monolayer SnSe is a good auxetic material. As the similar phenomenon was also observed in black phosphorus,^{15,18} which may be common in materials with such hinge-like structures. However, the negative Poisson's ratio of monolayer SnSe emerges between armchair (y) direction and perpendicular z direction, while that appears between zigzag (y) and perpendicular z directions for phosphorene. Besides, the absolute value of negative Poisson's ratio of monolayer SnSe is 6 times larger than phosphorene (-0.027).¹⁸ Thus the mechanism of negative Poisson's ratio in monolayer SnSe and phosphorene should be different, which may also be due to the strong nonbonding interaction in monolayer SnSe. Furthermore, a turning point in $\epsilon_z - \epsilon_x$ strain curve can be observed under 5% compressive strain along x direction, indicating a geometric phase transition, in which the space group of monolayer SnSe changes from Pmn21 (No. 31) to Pmmn (No. 59) (see supporting materials), behaving similarly with the geometric phase transition from Pnma (No. 62) to Cmcn (No. 63) in bulk SnSe under a high pressure²⁴. However, the corresponding transition stress for monolayer SnSe is about 1.6 GPa, while the critical hydrostatic pressure for bulk is about 10.5 GPa²⁴. Thus, a very low stress could induce the geometrical phase transition, which may be useful for manipulating the properties of monolayer SnSe. The stress-strain relations are given in the insets of Fig. 3, from which the Young's elastic modulus can be obtained as 24 GPa and 44 GPa along the x and y direction, respectively, showing a less anisotropic character than phosphorene⁴⁰ (44 GPa and 166 GPa). It is worth to note that monolayer SnSe is much more flexible than phosphorene and other isotropic 2D

materials, such as graphene⁴¹ (1000 GPa), h-BN⁴² (250 GPa), and MoS₂⁴³ (330 GPa), and may be the most flexible in the known 2D materials⁴⁴.

Strain effect on electronic properties of monolayer SnSe

Figure 4 presents the energy bands of monolayer SnSe under different uniaxial strains. The VBMs (V_X and V_Y) and the CBMs (C_X and C_Y) are marked by small filled and unfilled squares and circles, respectively. Obviously, when the compressive strain is increased along x direction, C_X moves down and V_Y moves up, leading to a shrinking indirect band gap; when the tensile strain is increased along x direction, C_X moves up and V_Y moves down, while V_X and C_Y are nearly fixed, leading to an intact indirect band gap. When the compressive strain is increased along y direction, C_X moves up and V_Y moves down, while V_X and C_Y are nearly fixed, leading to a nearly intact indirect band gap; when the tensile strain is increased along y direction, C_X moves down and V_Y moves up with the increase of the strain, leading to a shrinking indirect band gap. The strain effect on C_X , C_Y , V_X and V_Y can be seen in Fig. 3c and Fig. 3d. One may note that the compressive strain along y direction affects the same way as the tensile strain along x direction, and vice versa. This is understandable, as the intra-layer lattice parameters a and b are with positive Poisson's ratio, when a is compressed, b is elongated, and vice versa. Another interesting fact is that V_X is nearly always fixed whenever compressive and tensile strains are applied along x or y direction; C_Y acts similar when the tensile strain along x direction or the compressive strain along y direction is applied; while V_Y and C_X are always sensitive and nearly linear response to any strain, showing a weakly anisotropic response of electronic structures to the strain. Furthermore, from Fig. 3c and 3d, the colored areas marked by II and V correspond to the direct band gap, while I, III, IV and VI represent the indirect band gap. Thus, a strain-induced direct and indirect band gap transition can be observed. Notice that only a small compressive

stress along x direction (about 0.24 GPa) or a tensile stress along y direction (about 0.45 GPa) will make monolayer SnSe transit from an indirect gap to a direct band gap; when these strains continue to increase more than about 2.5% (about 1.14 GPa), the energy gap shrinks and transits from a direct one into an indirect one again. 10% compressive strain along x direction (4.5 GPa) and tensile strain (4.5 GPa) along y direction reduce the band gap to 0.3 and 0.6 eV, respectively. However, the compressive strain along y direction or the tensile strain along x direction almost does not affect the band gap. Therefore, a low stress could give rise to diverse electronic structures, which makes monolayer SnSe an excellent 2D semiconductor material for the strain band engineering^{45,46}. Such properties would also be very useful in nanoelectronics and optoelectronics.

The strain effect on the effective mass of charge carrier is studied as well. It is found that the compressive strain along x direction and the tensile strain along y direction will decrease the carrier effective mass, and the biaxial tensile strain will dramatically increase effective mass and induce noticeable anisotropy. See supporting materials for details. Using the deformation potential theory, the charge carrier mobility can be evaluated from carrier effective mass, deformation potential constant, and effective 2D elastic modulus, which are listed in Table I. Interestingly, while the effective mass of electron and hole are isotropic, the mobility are far from isotropic. We found that the hole mobility in monolayer SnSe is much larger than electron in both directions, and the highest hole mobility is 16680-18420 $\text{cm}^2\text{V}^{-1}\text{S}^{-1}$ along x direction, which is nearly one order higher than that along y direction (1600-1820 $\text{cm}^2\text{V}^{-1}\text{S}^{-1}$). Hence, monolayer SnSe will exhibit strong anisotropic p -type properties in electronic transport, which is consistent with the experimental work³¹. We also observed that the deformation potential constants along x (E_{1_x}) are dramatically smaller than that along y direction (E_{1_y}), and the

effective 2D elastic modulus along y direction (C_{2D_y}) is nearly double of that along x direction (C_{2D_x}), which are the origin of anisotropic carrier mobility. E_{l_x} is evaluated from the energy change of VBT (V_X) under proper strain along x direction. As can be seen in Fig. 4a, V_X is nearly fixed under different strain, thus it is consistent with the extremely small E_{l_x} and is responsible for an ultrahigh hole mobility along x direction. It also implies that the behavior of energy band under different strain can be viewed as an indicator of high carrier mobility. Since the deformation potential theory can only considered the scattering effect of longitudinal acoustical phonon, while other scattering mechanism such as optical phonons, impurities, etc. are not included, the experimentally observed carrier mobility may be not as high as calculated here. Note a high mobility in phosphorene along y direction was also predicted¹⁴, while in monolayer SnSe, it is dominate along x direction, which may be owing to different anisotropic electronic response to strain.

Conclusion

By means of first-principles calculation, the geometrical structure, mechanical, thermal transport and electronic properties of monolayer SnSe and the strain effect are systematically investigated. SnSe monolayer is a semiconductor with an indirect band gap of 1.45 eV and a hole mobility as high as $16000 \text{ cm}^2\text{V}^{-1}\text{S}^{-1}$. In contrast to phosphorene, which is the isoelectronic and a similar structure partner to monolayer SnSe and has strong anisotropic mechanical, electronic, and optical properties, we found that monolayer SnSe has nearly symmetric phonon and electronic band structures, leading to nearly isotropic lattice thermal conductivity and charge carrier effective mass, which can be attributed to the effectively symmetric square-like lattice structure. The strain effect on SnSe monolayer was also studied, showing that the geometric, mechanic and electronic properties are sensitive to the strain. A very low stress (1.6 GPa) along x direction can

induce a geometrical phase transition. Besides, a uniaxial strain will shift the extremes of different energy valleys asynchronously, giving rise to an indirect-direct band gap transition under a rather low stress (< 0.5 GPa). Although the effective mass of charge carrier is isotropic, the carrier mobility is anisotropic, which can be attributed to the anisotropic response to strain in monolayer SnSe. Furthermore, monolayer SnSe has an ultralow lattice thermal conductivity below $3 \text{ Wm}^{-1}\text{K}^{-1}$ and a large negative Poisson's ratio. Therefore, the rich properties of monolayer SnSe suggest that it should be an excellent 2D material candidate for nanomechanics, thermoelectrics and optoelectronics.

Methods

Most of the calculations are performed using Vienna *ab initio* simulation package (VASP)⁴⁷ with the generalized gradient approximation of Perdew-Burke-Ernzerhof (PBE)⁴⁸ for the exchange-correlation potential and a projector augmented wave (PAW)⁴⁹ method. The kinetic energy cutoff for plane wave functions is set to 700 eV and the energy convergence threshold is set as 10^{-5} eV. The Monkhorst-Pack k-meshes⁵⁰ of $15 \times 15 \times 5$ and $15 \times 15 \times 1$ are employed to sample the irreducible Brillouin zone of the bulk and finite layer SnSe, respectively. The shape and volume for each cell were fully optimized and the maximum force on each atom is less than $0.002 \text{ eV}/\text{\AA}$. The optB88-vdW functional⁵¹ is adopted to consider the van der Waals interactions. The modified Becke-Johnson (mBJ)⁵² method is adopted to calculate electronic band structures. The phonon dispersion is calculated using PHONOPY package⁵³ with the finite displacement method. The lattice thermal conductivity is calculated using ShengBTE code³⁶. The effective

masses are derived from the band structure. The carrier mobility in 2D materials are calculated using the equation ⁵⁴⁻⁵⁶:

$$\mu_{2D} = \frac{e\hbar^3 C_{2D}}{k_B T m_e^* m_d (E_l)^2}$$

where m_e^* is the effective mass for the conveyor direction and m_d is the average effective mass defined by the expression: $m_d = \sqrt{m_x^* m_y^*}$, T represents the temperature that is taken as 300K. E_l is the deformation potential constant that contains the VBM for hole and the CBM for electron along the conveyor direction, expressed as $E_l = \Delta V / (\Delta l / l_0)$. Here l_0 is the lattice constant along the conveyor direction, Δl is the distortion of l_0 , and ΔV is the energy change of the band with proper strain (the step is set as 0.5%). C_{2D} represents the effective 2D elastic modulus, and here we calculate the C_{2D} by the function:

$$C_{2D} = \frac{1}{S_0} \left. \frac{\partial^2 E}{\partial (l/l_0)^2} \right|_{l=l_0}$$

where E is the total energy after deformation, E_0 is the original total energy and S is the lattice volume at equilibrium for a 2D system.

FIGURES

Figure 1

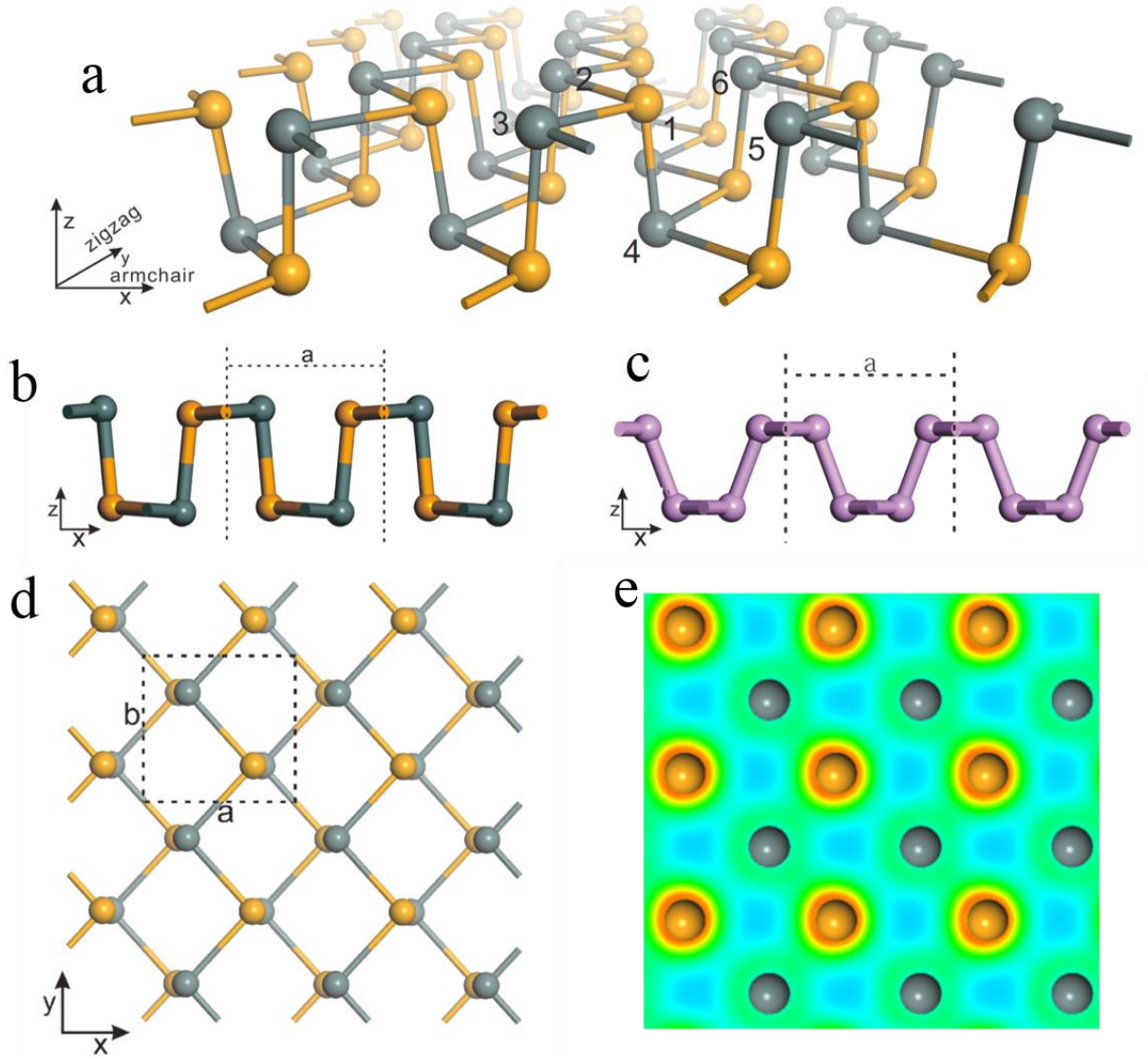


Figure 1 Schematic structures of monolayer SnSe. (a) Perspective view, (b) side view and (d) top view. Yellow balls denote Se atoms and gray balls denote Sn atoms. The numbers from 1 to 6 label the neighboring Sn and Se atoms. The primitive cell of monolayer SnSe is indicated by dashed lines, where a and b denote the lattice parameter in the x (armchair) and y (zigzag) direction, respectively. The side view of phosphorene (c) is included to compare with monolayer SnSe. The two-dimensional charge density of monolayer SnSe (e) is illustrated in the xy plane containing all Sn atoms.

Figure 2

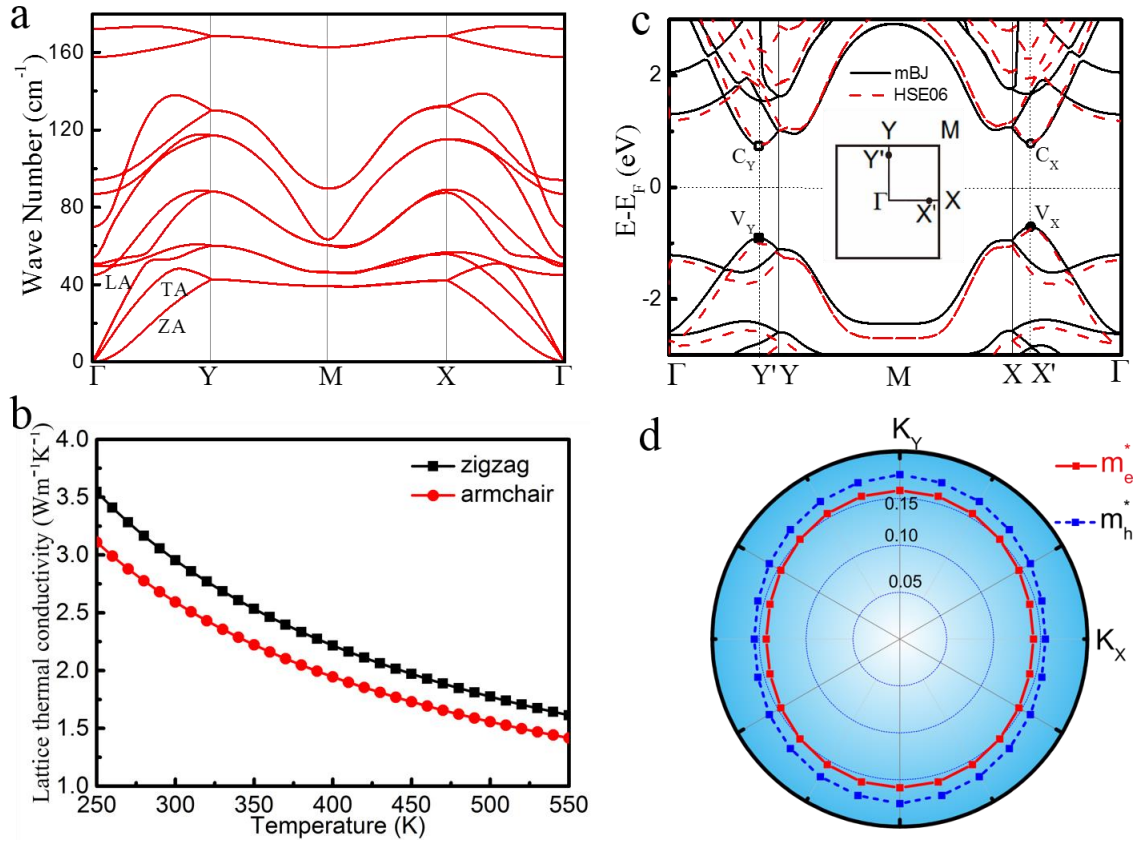


Figure 2 (a) The phonon dispersion for monolayer SnSe, where three acoustic phonon branches are indicated as LA, TA and ZA. (b) The lattice thermal conductivity of monolayer SnSe in the armchair (x) and zigzag (y) directions, respectively. (c) The band structure of monolayer SnSe, where black line represents the calculation with mBJ functional and red line with HSE06 method. The CBM and VBM for the band structure are marked as C_Y , C_X and V_Y , V_X , respectively. (d) The effective mass for electrons and holes.

Figure 3

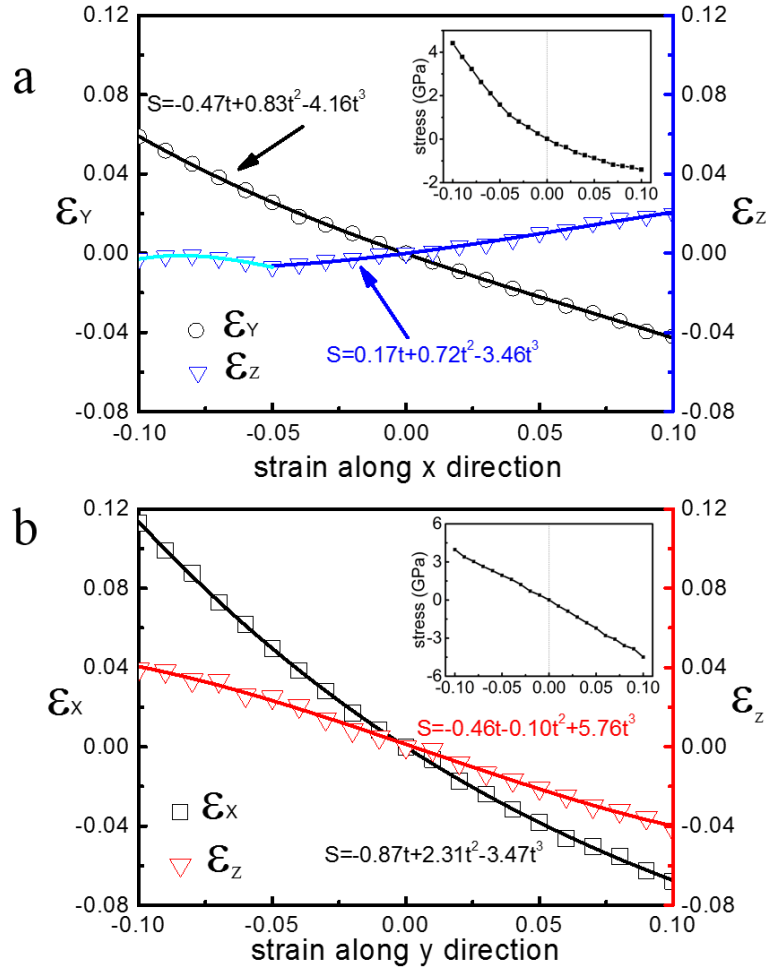


Figure 3 The mechanical response of monolayer SnSe under uniaxial strain along x (a) and y (b) directions. Strain is defined as $s = (l - l_0)/l_0$, where $l = a, b, c$ represent the lattice parameters (thickness for c) along x, y, z directions under strain, respectively, and $l_0 = a_0, b_0, c_0$ are the corresponding original lattice constants (thickness for c_0) without strain. The positive (or negative) s means a tensile (or compressive) strain, while $s = 0$ corresponds the case without strain. The Poisson's ratio can be obtained by fitting $s = -\nu_1 t + \nu_2 t^2 + \nu_3 t^3$, where t is the strain along the x or y direction, t is the strain along lateral direction, and ν_1 could be regarded as the Poisson's ratio. The corresponding stress-strain relations in x and y directions are shown in the upper right insets.

Figure 4

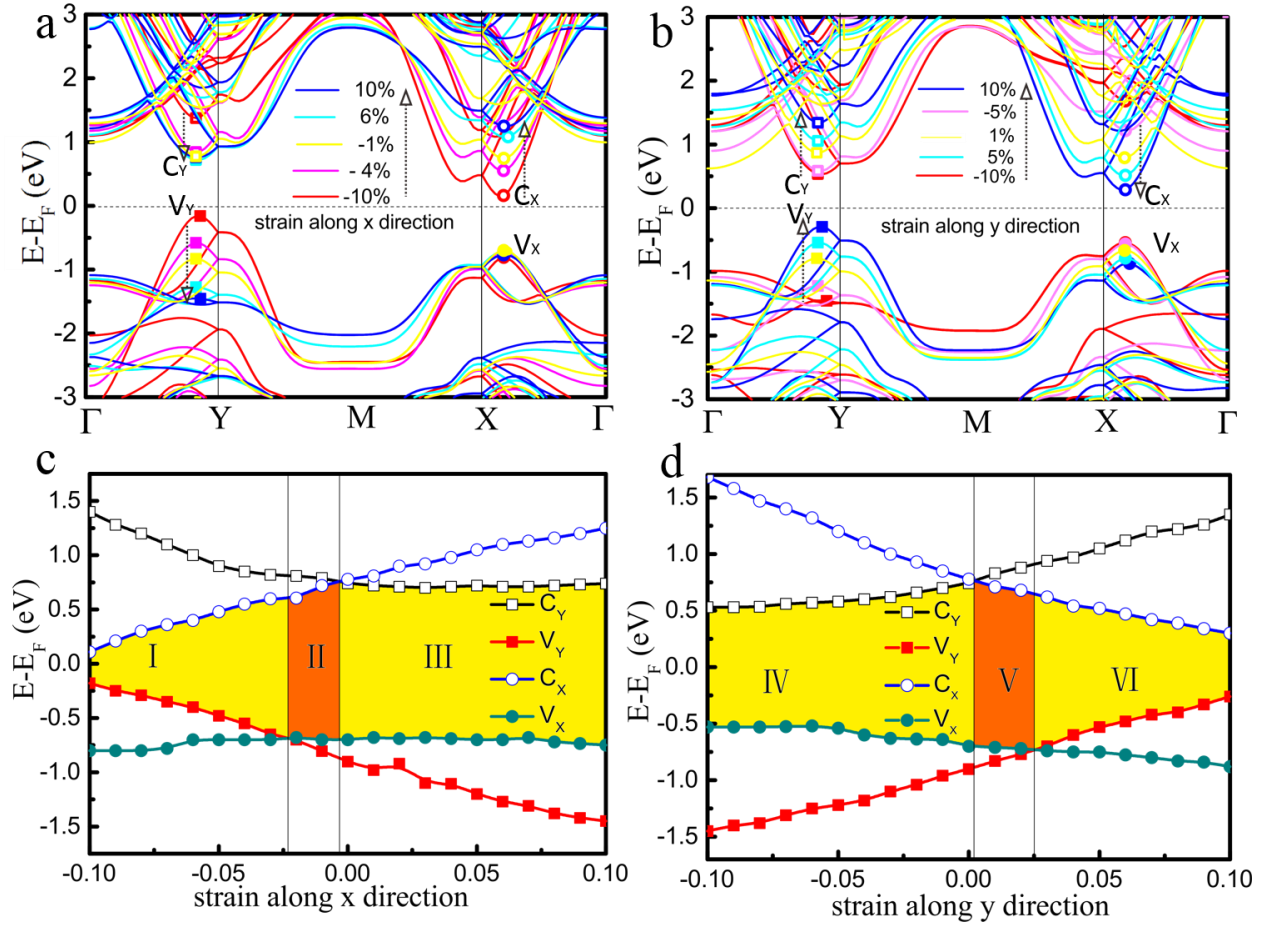


Figure 4 Band structure of monolayer SnSe calculated by mBJ method under uniaxial strain from -10% to 10% along x (a) and y (b) directions. The CBM and VBM in the band structure are marked by C_Y , C_X and V_Y , V_X , respectively. The energies of C_Y , C_X , V_Y and V_X as a function of strain in the x (c) and y (d) directions are plotted. The indirect band gap appears in regions I, III, IV and VI, and the direct band gap appears in the regions II and V. The transition from an indirect gap to a direct gap can be determined by the energy crossover.

TABLES.

Table 1. The effective mass and mobility of charge carriers in monolayer SnSe

Carrier type	m_x^*/m_0	m_y^*/m_0	E_{l_x}	E_{l_y}	C_{2D_x}	C_{2D_y}	μ_{2D_x}	μ_{2D_y}
	Γ -X	Γ -Y	(eV)		(Jm ⁻²)		(10 ³ cm ² V ⁻¹ S ⁻¹)	
electron	0.143	0.158	1.62 ± 0.05	4.5 ± 0.04	13.46	26.58	4.80-5.42	1.14-1.20
hole	0.155	0.175	0.8 ± 0.02	3.4 ± 0.12	13.46	26.58	16.68-18.42	1.60-1.82

Table 1 The predicted effective mass and mobility of carriers in monolayer SnSe. m_x^* and m_y^* are effective mass in Γ -X and Γ -Y directions, respectively. E_{l_x} (E_{l_y}) and C_{2D_x} (C_{2D_y}) represent the deformation potential constant and effective 2D elastic modulus for x (y) direction. μ_{2D_x} and μ_{2D_y} denote the carrier mobility in x and y direction, respectively. Note that the calculated effective 2D elastic modulus are consistent with the Young's modulus evaluated from stress-strain relations. (See supporting materials)

Supporting Information.

The supporting materials are available at DOI: ***

Corresponding Author

*Email: (Q.-B.Y.) yan@ucas.ac.cn.

*Email: (G.S.) gsu@ucas.ac.cn.

ACKNOWLEDGMENT

The authors thank Dr. Li-Zhi Zhang of University of Utah, Prof. Wei Ji of RUC and Prof. Zhen-Gang Zhu of UCAS for helpful discussions. All calculations are performed on Nebulae (DAWN6000) in National Supercomputing Center in Shenzhen and MagicCube (DAWN5000A) in Shanghai Supercomputer Center, China. This work is supported in part by the NSFC (Grant No. 11004239), the MOST (Grant No. 2012CB932901 and No.2013CB933401) of China, and the fund from CAS.

REFERENCES

- [1] Geim, A. K.; Novoselov, K. S. *Nature Mater.* **2007**, 6, 183
- [2] Novoselov, K. S.; Geim, A. K.; Morozov, S. V.; Jiang, D.; Katsnelson, M. I.; Grigorieva, I. V.; Dubonos, S. V.; Firsov, A. A. *Nature* **2005**, 438, 197
- [3] Zhang, Y.; Tan, Y.-W.; Stormer, H.; L.; Kim, P. *Nature* **2005**, 438, 201
- [4] Geim, A. K.; Novoselov, K. S. *Science* **2009**, 324, 1530
- [5] Coleman, J. N.; Lotya, M.; O'Neill, A.; Bergin, S. D.; King, P. J.; Khan, U. et al., *Science* **2011**, 331, 568
- [6] Liu, L.; Feng, Y. P.; Shen, Z. X. *Phys. Rev. B* **2003**, 68, 104102
- [7] Levendorf, M. P.; Kim, C. J.; Brown, L. Huang, P. Y.; Havener, R. W.; Muller, D. A.; Park, J. *Nature* **2012**, 488, 627
- [8] Wang, Q. H.; Kalantar-Zadeh, K.; Kis, A.; Coleman, J. N.; Strano, M. S. *Nature Nano* **2014**, 7, 699
- [9] Geim, A. K.; Grigorieva, I. V. *Nature* **2013**, 499, 419
- [10] Vogt, P.; Padova, P. D.; Quaresima, C.; Avila, J.; Frantzeskakis, E.; Asensio, M. C.; Resta, A.; Ealet, B.; Lay, G. L. *Phys. Rev. Lett.* **2012**, 108, 155501

- [11] Houssa, M.; Scalise, E.; Sankaran, K.; Pourtois, G.; Afanas'ev, V. V.; Stesmans, A. Appl. Phys. Lett. **2011**, 98, 223107
- [12] Bianco, E.; Butler, S.; Jiang, S.; Restrepo, O. D.; Windl, W. G. J. E. ACS Nano **2013**, 7, 4414
- [13] Xu, M.-S.; Liang, T.; Shi, M.-M.; Chen, H.-Z. Chem. Rev. **2013**, 113, 3766
- [14] Qiao, J.; Kong, X.; Hu, Z. X.; Yang, F.; Ji, W. Nat. Commun. **2014**, 5, 4475
- [15] Qin, G.Z.; Yan, Q.-B.; Qin, Z.-Z.; Yue, S.Y.; Zheng, Q.-R.; Su, G. Sci. Rep. **2014**, 4, 6946
- [16] Qin, G.Z.; Yan, Q.-B.; Qin, Z.-Z.; Yue, S.Y.; Hu, M.; Su, G. Phys. Chem. Chem. Phys. **2014**, 17, 4854
- [17] Fei, R.; Yang, L.; Nano Lett. **2014**, 14, 2884
- [18] Jiang, J.W.; Park, H. S. Nat. Commun. **2014**, 5, 4727
- [19] Rodin, A. S.; Carvalho, A.; Castro Neto, A.H. Phys. Rev. Lett. **2014**, 112, 176801
- [20] Peng, X.; Wei, Q.; Copple, A.; Phys. Rev. B **2014**, 90, 085402
- [21] Liu, H.; Neal, A.T.; Zhu, Z.; Luo, Z.; Xu, X.-F.; Tománek, D.; Ye, P. D. ACS Nano **2014**, 8, 4033
- [22] Chattopadhyay, T.; Pannetier, J. and Schnering, H.G.V. J. Phys. Chem. Solids **1986**, 47, 879
- [23] Lefebvre, I.; Szymanski, M.A.; Olivier-Fourcade, J. and Jumas, C. Phys. Rev. B **1998**, 58, 1896
- [24] Loa, I.; Husband, R. J.; Downie, R. A.; Popuri, S. R.; Bos, J.-w. G. J. Phys.: Condens. Matter **2015**, 27, 072202
- [25] Shi, G.-S.; Kioupakis, E.; J. Appl. Phys. **2015**, 117, 065103
- [26] Zhao, L.-D.; Lo, S.-H.; Zhang, Y.-S.; Sun, H.; Tan, G.-J.; Uher, C.; Wolverton, C. David, V.P. and Kanatzidis, M.G. Nature **2014**, 508, 373
- [27] Chun, D.; Walser, R.M.; Bene, R. W.; Courtney, T. H.; Appl. Phys. Lett. **1974**, 24, 479
- [28] Franzman, M. A.; Schlenker, C.W.; Thompson, M. E.; Brutchey, R. L. J. Am. Chem. Soc. **2010**, 132, 4060
- [29] Antunez, P.Z.; Buchley, J.J. and Brutchey, R.L. Nano scale **2011**, 3, 2399
- [30] Li, L.; Chen, Z.; Hu, Y.; Wang, X.; Zhang, T.; Chen, W.; Wang, Q.; J. Am. Chem. Soc. **2013**, 135, 1213
- [31] Zhao, S.; Wang, H.; Y. Zhou.; Liao, L.; Jiang, Y.; Yang, X.; Chen, G.; Lin, M.; Wang, Y.; Peng, H.; Liu, Z. Nano Res. **2015**, 8, 288
- [32] Wang, C.; Xia, Q. -L.; Nie, Y.-Z.; Guo, G.-H.; J. Appl. Phys. **2015**, 117, 124302
- [33] Cai, Y.-Q.; Ke, Q.-Q.; Zhang, G.; Feng, Y.-P.; Sheng, V. B.; Zheng, Y.-W.; Adv. Funct. Mater. **2015**, 25, 2230
- [34] Xia, F.-N.; Wang, H.; Jia, Y. -C.; Nat. Commun. **2014**, 4, 4458
- [35] Tran, V.; Soklaski, R.; Liang, Y.-F.; Yang, L. Phys. Rev. B **2014**, 89, 235319
- [36] Li, W.; Carrete, J.; Katcho, N. A.; and Mingo, N.; Comput. Phys. Commun., **2014**, 185, 1747
- [37] Cai, Y.Q.; Lan, J.H.; Zhang G.; and Zhang Y.-W. Zhang, Phys. Rev. B **2014**, 89, 035438
- [38] Cepellotti, A.; Fugallo, G.; Paulatto, L.; Lazzeri, M.; Mauri, F.; and Marzari, N.; Nature Commu. **2015**, 6, 6400
- [39] Taube, A.; Judek, J.; Łapińska, A.; and Zdrojek, M.; ACS Appl. Mater. Interfaces, **2015**, 7, 5061–5065
- [40] Wei, Q.; and Peng, X.H., Appl. Phys. Lett. **2014**, 104, 251915
- [41] Lee, C.; Wei, X. D.; Kysar, J. W.; and Hone, J. Science **2008**, 321, 385–388
- [42] Song, L.; Ci, L. J.; Lu, H.; Sorokin, P. B.; et al., Nano Lett. **2010**, 10, 3209–3215

- [43] Castellanos-Gomez, A.; Poot, M.; Steele, G. A.; et al., Adv. Mater. **2012**, 24, 772–775
- [44] Andrew, R. C.; Mapasha, R. E.; Ukpong, A. M.; and Chetty. N., Phys. Rev. B **2012**, 85, 125428
- [45] Feng, J.; Qian, X.F.; Huang C.-W.; and Li, J.; Nature Photonics **2012**, 6, 866–872
- [46] Akinwande, D.; Petrone, N.; and Hone, J.; Nature Comm. **2014**, 5, 5678
- [47] Kresse, G.; Furthmüller, J.E. Phys. Rev. B **1996**, 54, 11169
- [48] Perdew, J. P.; Burke, K.; Ernzerhof, M. Phys. Rev. Lett. **1996**, 77, 3865
- [49] Kresse, G.; Joubert, D.; Phys. Rev. B **1999**, 59, 1758
- [50] Monkhorst, H. J.; Pack, J. D. Phys. Rev. B **1976**, 13, 5188
- [51] Klimes, J.; Bowler, D. R.; Michaelides, A.; Condensed Matter **2010**, 22, 022201
- [52] Tran, F.; Blaha, P.; Phys. Rev. Lett. **2009**, 102, 226401
- [53] Togo, A.; Oba, F.; Tanaka, I. Phys. Rev. B, **2008**, 78, 134106
- [54] Bruzzone, S.; Fiori, G.; Apple. Phys. Lett. **2011**, 99, 2108 (2011)
- [55] Takagi, S. -i.; Toriumi, A.; Iwase, M.; Tango, H.; IEEE Trans. Electr. Dev. **1994**, 41, 2357
- [56] Fiori, G.; Iannaccone, G.; Proc. IEEE **2013**, 101, 1653